Silent central modes of the superionic conductor $LiKSO_4$ studied by means of hyper-Raman scattering: Evidence of coupling between lithium-ion conduction and sulfate-ion rotation

S. Shin and Y. Tezuka
Synchrotron Radiation Laboratory, Institute for Solid State Physics, The University of Tokyo, 3-2-1 Midori-cho, Tanashi, Tokyo 188, Japan

A. Sugawara and M. Ishigame
Research Institute for Scientific Measurements, Tohoku University, 2-1-1 Katahira, Sendai, Miyagi 980, Japan
(Received 13 June 1991)

Relaxational central modes due to the rotational Brownian motion of the sulfate ions are measured by hyper-Raman scattering in $LiKSO_4$ crystal. The B_{1u} relaxational mode is the rotational mode about the c axis. This is a silent mode, which is inactive for Raman and infrared measurements. The infrared-active E_{1u} relaxational modes are also found, which are the rotational modes about the a and b axes. Since the anisotropy of the Li^+-ion conductivities is well elucidated by the ratio of B_{1u}- and E_{1u}-rotational relaxation times, the coupling between sulfate-ion rotation and Li^+-ion migration is strongly supported. Relaxational central modes are also found in Raman scattering. A comparison between the Raman and hyper-Raman spectra shows that interactions between sulfate ions are strong in rotations about the a and b axes. However, they are weak for rotations about the c axis.

I. INTRODUCTION

A large number of $ABSO_4$-type sulfate compounds (A,B=Li, Na, K, Cs, Rb, Ag, NH_4, and H) has been studied by various experiments, due to interest in their sequence of phase transitions and the existence of incommensurate phase transitions.[1] Many different phase transitions have been proposed under various experimental techniques. However, the existence of some phases is under controversy and the crystal structures of many phases are not known. Most of these phase transitions which occur are due to the slight tilt of SO_4 tetrahedra. Obviously, the interactions between octupole moments is important in these phase transitions, because a SO_4 tetrahedron is an octupole moment itself. If a SO_4 tetrahedron is not distorted, it has only an octupole moment and does not have dipole and quadrupole moments. Furthermore, it is noted that SO_4 tetrahedra in most materials rotate in the high-temperature phases and that these materials become superionic conductors of lithium ions in the high-temperature phases. Thus, it has been proposed[1,2] that there is a coupling between SO_4^{2-}-ion and Li^+-migration. This mechanism is called "paddle-wheel" or "cog-wheel" mechanism. There is, however, no consensus on a mechanism for this coupling.

Lithium potassium sulfate ($LiKSO_4$)has been the most studied of all the $ABSO_4$-type sulfate compounds, because large single crystals are easily obtainable and they are stable in air. Furthermore, this crystal is not easily broken by the phase transition irrespective of the first-order phase transition. Thus, $LiKSO_4$ is selected as the most suitable material to study by hyper-Raman and Raman scattering in this paper.

Many studies[3-14] of the structure of $LiKSO_4$ have been made. $LiKSO_4$ has a hexagonal structure at room temperature belonging to the space group $P6_3(C_6^6)$ with two molecular formulas as shown in Fig. 1(a). Lattice constants of this crystal are a=5.147 Å and c=8.633 Å. The slight tilts of SO_4 tetrahedra around the c axis give rise to a number of phases at low temperatures in $LiKSO_4$.

By the structural studies of $LiKSO_4$, SO_4 tetrahedra rotate around the a and b axes as well as the c axis in the high-temperature phase above 670 °C up to the melting point at around 720 °C. Thus, the orientation of SO_4 tetrahedra becomes disordered. It is assumed that SO_4

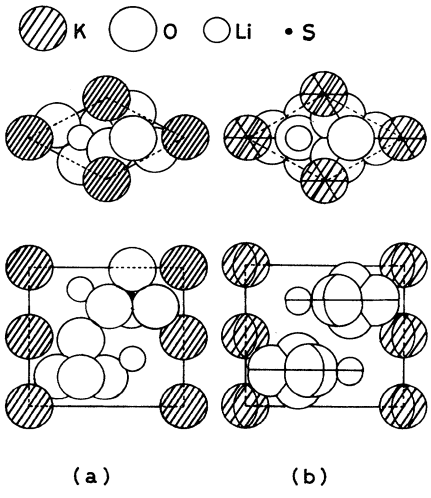

FIG. 1. Crystal structure of $LiKSO_4$ and K_2SO_4 projected onto the a-b plane and along the c axis at the room-temperature phase (a) and high-temperature phase (b), respectively. The crystal structure in the high-temperature phase is said to be isomorphic to K_2SO_4.

tetrahedra rotate dynamically so that the random distribution of their orientations is not static. The crystal structure of $LiKSO_4$ at high temperature is assumed to be isomorphic with that of α-K_2SO_4, which belongs to the space group D_{6h}^4, where the SO_4 tetrahedra are also disordered. Figure 1(b) is the crystal structure[15] of α-K_2SO_4. The lithium ions of $LiKSO_4$ are supported to be in the site of the potassium(2) ion of K_2SO_4. It is known that the positions of potassium(1) and potassium(2) ions are slightly disordered for K_2SO_4 as shown in Fig. 1(b). Potassium(2) ions have two positions and potassium(1) ions have two positions, which may be a result of the orientation of SO_4 tetrahedra. That is, potassium(2) ions (Li^+ ions in $LiKSO_4$) move along the c axis according to the change of the direction of SO_4^{2-} tetrahedra along c axis and the potassium(1) ions move along the a and b axes according to the rotation of SO_4^{2-} tetrahedra about the c axis. However, to date such displacements have not been confirmed for $LiKSO_4$.

In the intermediate temperature range between 435° and 670 °C, it is said that the orientations of SO_4^{2-} tetrahedra are partially disordered. Furthermore, there is a controversy about the symmetry of the crystal structure in this phase. It is said that it belongs to the orthorhombic symmetry.[13] Furthermore, an incommensurate structure[6] between 439 °C and 662 °C is suggested. However, the existence of this incommensurate phase is controversial.

In this paper, Raman and hyper-Raman scattering of $LiKSO_4$ are measured. The Raman (R) process is the two-photon process and the hyper-Raman (HR) process is the three-photon process, as indicated by R and HR in Fig. 2(b). ω_i is the frequency of the incident laser light and ω_0 is the frequency of the scattered light. ω_p is the energy of the elementary excitation, such as the phonon frequency. When the laser light with electric field E is introduced into the crystal, light scattering will occur by the following process:

$$P_i=\alpha_{ij}E_j+\beta_{ijk}E_jE_k+\gamma_{ijkl}E_jE_kE_l+\cdots,$$

where the first term is the Raman process, the second term is the hyper-Raman process, and the third term of the four-photon process is a higher-order process than hyper-Raman, which will be named second hyper-Raman process (SHR) in this paper. α_{ij}, β_{ijk}, and γ_{ijkl} are the Raman, hyper-Raman, and second hyper-Raman tensors. Each light scattering is caused by the fluctuations of each tensor due to the ion displacements. Since the bases of these tensors are written by polynomials of two, three, and four variables, the fluctuations of these tensors correspond to the fluctuations of quadrupole, octupole, and hexadecapole moments. Furthermore, hyper-Raman is active for the fluctuation of dipole moment and second hyper-Raman is active for the fluctuation of quadrupole moment. The selection rules of Raman, hyper-Raman, and second hyper-Raman scattering as well as infrared measurement are summarized in Fig. 2(a). When the materials have centrosymmetry, hyper-Raman and infrared modes are the ungerade mode. Raman and second hyper-Raman modes are the gerade modes. When they do not have centrosymmetry, the selection rule of these modes overlaps each other.

Figure 3 shows the multipole moments of 2^l according to the l and m of the spherical harmonics $Y_{lm}(\theta,\phi)$. $l=1$, 2, and 3 give the dipole, quadrupole, and octupole moments, respectively. The fluctuation of such a multipole moment in the material is the origin of the light scattering. If the material contains the molecule ion whose shape is a multipole moment, the selection rule of the fluctuation of each molecule is easily understood. For example, the H_2O molecule has $l=1$, the CS_2 molecule has $(l,m)=(2,0)$, the CCl_4 molecule has $(l,m)=(3,2)$, the NH_3 molecule has $(l,m)=(3,3)$, and the SF_6 molecule has

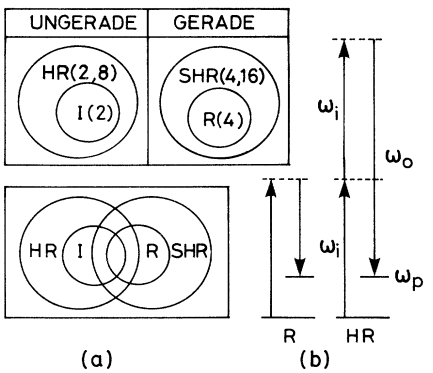

FIG. 2. (b) is the schematic diagram of the Raman (R) and hyper-Raman (HR) processes. ω_i is the frequency of the incident laser light. ω_0 is the frequency of the scattered light. (a) show the selection rule of R, HR, infrared (I), and second-hyper Raman (SHR) measurements.

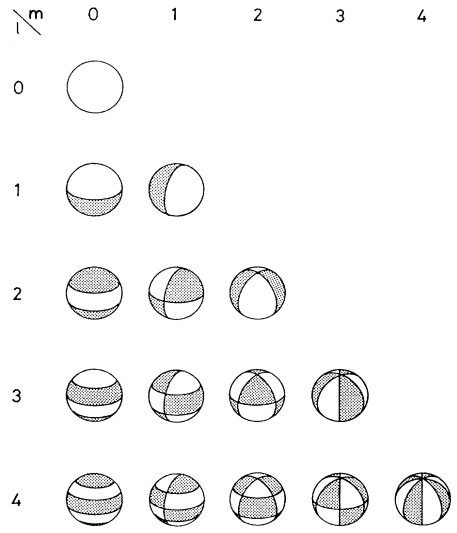

FIG. 3. Multipole moments of 2^l according to the l and m of the spherical function $Y_{lm}(\theta,\phi)$.

$(l,m)=(4,3)$. The rotational Brownian motion of each molecule in the liquid or the solid will give the central modes with the clear selection rule. That is, infrared measurement is active for the H_2O molecule. Raman scattering is active for the CS_2 molecule. Hyper-Raman scattering is active for the CCl_4 and NH_4 as well as the H_2O molecule. These rotational motions will give the silent mode. Second hyper-Raman scattering is active for the SF_6 as well as the CS_2 molecule. This gives the silent mode for the Raman, infrared, and hyper-Raman measurements.

The aim of this paper is to confirm the rotation of the SO_4 tetrahedra. This motion will give the central modes in the spectra. Since a SO_4^{2-} tetrahedron is an octupole moment itself, the rotational fluctuations of the SO_4^{2-} ion should be a silent central mode. The silent central mode has hitherto not been found. Thus, the aim of this paper is to find the silent central mode by means of hyper-Raman scattering. Another aim of this paper is to confirm the coupling mechanism of SO_4-ion rotation and Li-ion conduction by means of hyper-Raman and Raman scattering. Li-ion conduction will be determined by electrical-conductivity measurements.

The hyper-Raman tensors [B_{1u}, $E_{1u}(X)$, and $E_{1u}(Y)$] in the D_{6h} symmetry which is used in this paper are given as follows:

$$B_{1u}: \begin{bmatrix} c & -c & 0 & 0 & 0 & 0 \\ 0 & 0 & 0 & 0 & 0 & -c \\ 0 & 0 & 0 & 0 & 0 & 0 \end{bmatrix}, \quad E_{1u}(X): \begin{bmatrix} e & e/3 & f & 0 & 0 & 0 \\ 0 & 0 & 0 & 0 & 0 & e/3 \\ 0 & 0 & 0 & 0 & f & 0 \end{bmatrix}, \quad E_{1u}(Y): \begin{bmatrix} 0 & 0 & 0 & 0 & 0 & e/3 \\ e/3 & e & f & 0 & 0 & 0 \\ 0 & 0 & 0 & f & 0 & 0 \end{bmatrix}.$$

The B_{1u} mode is the silent mode which is inactive for Raman and infrared measurements. $E_{1u}(X)$ and $E_{1u}(Y)$ modes are active for both infrared and hyper-Raman measurements. A_{1g}, E_{1g}, and E_{2g}, modes which are active for Raman measurements, are measured. These Raman tensors are generally available in standard textbooks.

II. EXPERIMENTAL

Single crystals of $LiKSO_4$ were grown at 32 °C by slow evaporation from an equimolecular aqueous solution containing Li_2SO_4 and K_2SO_4. Hexagonal single crystals of about $15\times15\times7$ mm^3 were obtained for a month.

Complex impedance was measured by an *LCR* meter (HP model 4274A) which covers the frequency range from 10 kHz to 10 MHz. Direct current conductivities are obtained by the Cole-Cole plot analysis of complex impedance. A single crystal was cut in a rectangular shape with dimensions of $1.35\times3.30\times5.35$ mm^3. Pt paste was used as electrode.

An acoustic Q-switched Nd-YAG laser was used as a light source of hyper-Raman scattering. The peak power of the pulse was about 20 kW at 1 kHz. A single monochromator (HR320, Jobin Yvon) was used with a spectral resolution of 5.2 cm^{-1}. As a detector, PIAS (photon-counting two-dimensional image acquisition system, Hamamatsu Photonics K.K.) was used.

In the case of Raman scattering, an argon-ion laser was used. A double grating monochromator (CT1000D, JASCO) was used with the resolution of about 1.2 cm^{-1}.

III. RESULTS

A. Electrical conductivity

The temperature dependence of the electrical conductivity of $LiKSO_4$ above 600 °C is shown in Fig. 4. Closed circles ($\sigma_\parallel$) are the conductivities parallel to the c axis and open circles ($\sigma_\perp$) are those perpendicular to the c axis. A discontinuous increase of conductivity occurs at T_{c1} around 687 °C by about one order of magnitude, which corresponds to the phase transition from partial disorder to total disorder of the orientation of SO_4 tetrahedra. An anisotropy of the electrical conductivities of $LiKSO_4$ in the high-temperature phases has been found in the measurements. $\sigma_\parallel$ is always higher than $\sigma_\perp$ by about a factor of 1.28,

$$\sigma_\parallel/\sigma_\perp=1.28 .$$

That is, Li-ion migration is easier along the c axis than

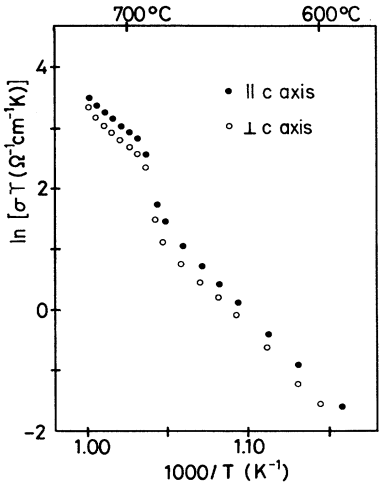

FIG. 4. Electric conductivities of $LiKSO_4$ along (∥) and perpendicular (⊥) to c axis.

perpendicularly to the c axis.

It is clearly found from Fig. 4 that the conductivities follow the Arrhenius relation,

$$\sigma T = A \exp(-\Delta/kT) \ . \quad (1)$$

The activation energies Δ are obtained to be 1.8 eV in the high-temperature phase. Since the conductivities are rather high at high temperature, one may call this crystal a superionic conductor. However, it is curious that the conductivity is rather high irrespective of the high activation energy. The ionic conductivities of $LiKSO_4$ have been also measured perpendicularly to the c axis by Pimenta *et al.*[16,17] from the room-temperature phase to the highest-temperature phase. Their results are rather consistent with our results in the intermediate-temperature phase but the activation energy and the conductivity seem to be high in the high-temperature phase. In Refs. 16 and 17, the conductivities also jump at the phase transitions of T_{c2} around 435 °C where the orientations of SO_4^{2-} tetrahedra are partially disordered from the ordered orientations. It is clear that the ionic conductivity is closely related with the SO_4^{2-} rotation.

B. Hyper-Raman scattering

Because hyper-Raman scattering of $LiKSO_4$ is very weak (about 2.8 counts/h channel) even in the strongest scattering configuration, it took about several days to obtain one spectrum. We measured the spectra in all configurations. However, the hyper-Raman spectra can be measured only for the central modes in $Z(XX,X)Y$, $Z(YY,X)Y$, and $Z(YY,Y)X$ configurations and cannot be measured in the other configuration. In the case of lattice modes, the spectra are too weak to be observed in any configurations.

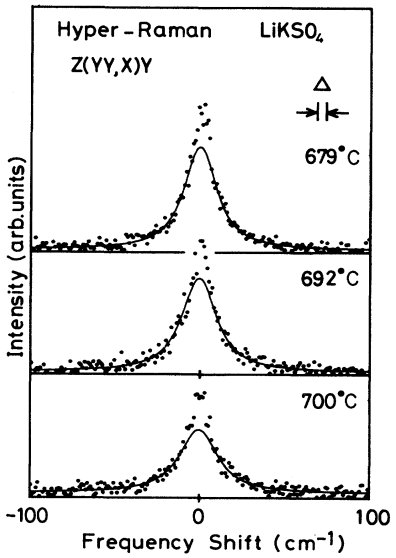

FIG. 6. Hyper-Raman spectra measured in the $Z(YY,X)Y$ configuration in the high-temperature phase. The solid lines are the calculated Lorentzian line shapes.

Figure 5 shows the central modes of $LiKSO_4$ in both $Z(XX,X)Y$ and $Z(YY,X)Y$ configurations at the same temperature. The full half widths are 26.0 and 22.4 cm^{-1} in $Z(XX,X)Y$ and $Z(YY,X)Y$ configurations, respectively. Considering the hyper-Raman tensors in D_{6h} symmetry, both spectra consist of B_{1u} and E_{1u} modes. The intensity of the latter is weaker by $\frac{1}{9}$ than that of the former

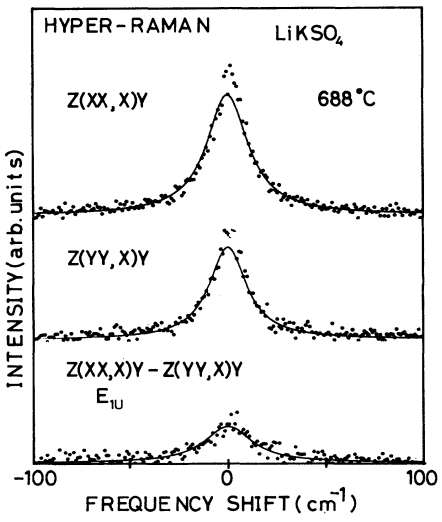

FIG. 5. Hyper-Raman scattering at 688 °C in the $Z(XX,X)Y$ and $Z(YY,X)Y$ configurations. The spectra in the lowest part is the E_{1u} mode, which is obtained by the subtraction of $Z(YY,X)Y$ from $Z(XX,X)Y$ spectra.

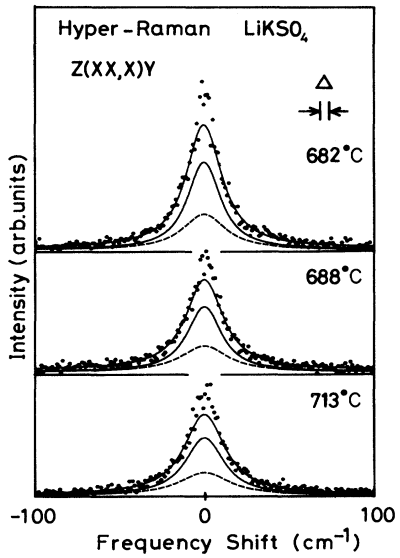

FIG. 7. Temperature dependence of the hyper-Raman spectra in the $Z(XX,X)Y$ configuration. The upper solid line is the summation of two Lorentzian line shapes. The dashed line is the E_u mode and the solid line is the B_{1u} mode.

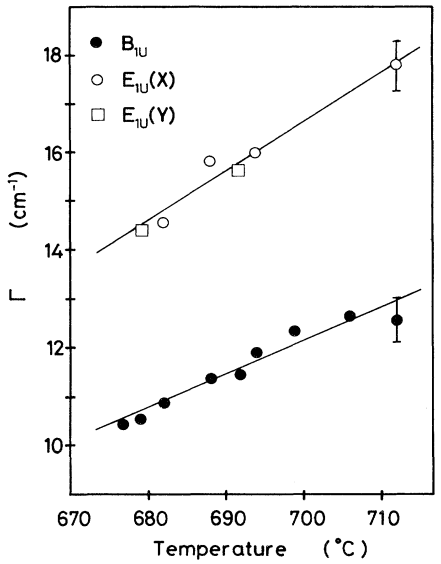

FIG. 8. Temperature dependences of linewidths of the central modes of E_{1u} (open circles and squares) and B_{1u} (closed circles) modes measured by hyper-Raman scattering of $LiKSO_4$.

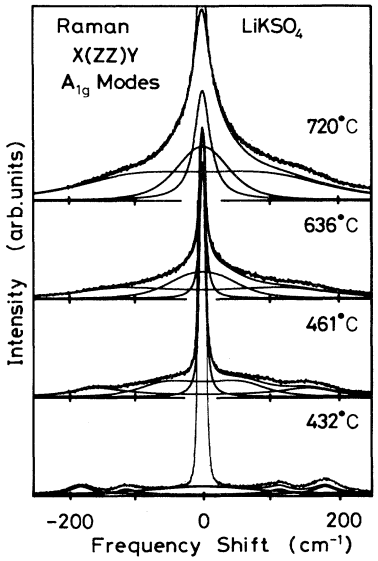

FIG. 9. Temperature dependence of A_{1g} Raman spectra $LiKSO_4$ in the $X(ZZ)Y$ configuration. The solid lines show the deconvoluted spectra by the central mode and damped lattice modes. The upper solid lines are the summation of these spectra.

in the E_{1u} mode, while the intensity of the B_{1u} mode is the same for both scattering. When the former is spectrum subtracted from the latter, only the E_{1u} mode remains as shown in Fig. 5. The full half width of the E_{1u} central mode is 31.7 cm^{-1}. Thus, the central mode in $Z(XX,X)Y$ and $Z(YY,X)Y$ configurations belongs mainly to the B_{1u} mode, though it overlaps with the $E_{1u}(X)$ mode.

The B_{1u} mode in D_{6h} symmetry is the silent mode. The silent central mode is found for the first time in $LiKSO_4$ by means of hyper-Raman scattering. This mode is due to the fluctuation of SO_4^{2-} tetrahedron, which is an octupole moment itself.

Considering the hyper-Raman tensors in D_{6h} symmetry, $Z(YY,Y)X$ configuration shows the $E_{1u}(Y)$ mode alone. $Z(XX,Y)X$ scattering also should show the $E_{1u}(Y)$ mode. Since the latter scattering is weaker by $\frac{1}{9}$ than that of former, it cannot be found because of its weak intensity.

Figures 6 and 7 show the central modes seen in the $Z(YY,X)Y$ and $Z(XX,X)Y$ spectra. The intensity decreases and the linewidth increases as the temperature becomes high. The solid lines are Lorentzians which are given by the following equation:

$$I(\omega)=A\,[n(\omega)+1]\chi(0)\frac{\tau}{1+(\omega\tau)^2}\ . \tag{2}$$

Here, τ is the relaxation time and $\chi(0)$ is the static susceptibility. The full half width is given by τ^{-1}. $n(\omega)$ is the Bose-Einstein factor, which approaches $kT/\hbar\omega$ at high temperature. The line-shape analysis of $I(\omega)\omega^2$ following Ref. 18 was performed and the spectral line shape is confirmed to be the Lorentzian but not the overdamped lattice mode.

The temperature dependences of full half width of B_{1u} and E_{1u} modes are summarized in Fig. 8. It is found that both are proportional to the temperature.

C. Raman scattering

Low frequency Raman spectra in $X(ZZ)Y$, $X(ZX)Y$ and $X(YX)Y$ configurations are shown in Figs. 9, 10, and 11, respectively. By a factor group analysis of the C_6^6

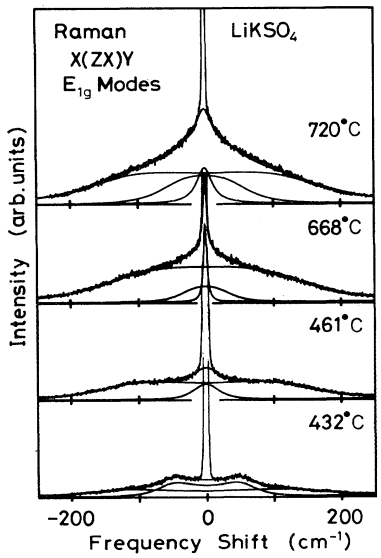

FIG. 10. Temperature dependence of E_{1g} Raman spectra of $LiKSO_4$ in the $X(ZX)Y$ configuration.

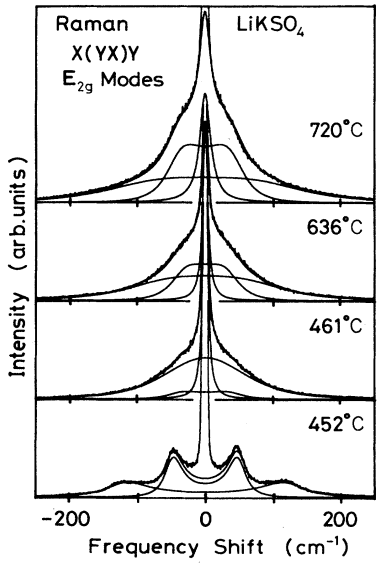

FIG. 11. Temperature dependence of E_{2g} Raman spectra of $LiKSO_4$ in the $X(YX)Y$ configuration.

space group of the room-temperature phase, Raman-active lattice modes are $3A+3E_1+4E_2$ modes. These modes become A_{1g}, E_{1g}, and E_{2g} modes, respectively at the high-temperature phase. Lithium modes[19] of $A+E_1+E_2$ modes exist in the highest-energy region around 400 cm^{-1}. Thus, all $2A+2E_1+3E_2$ modes should be seen in this energy region. All of these modes are found in the Raman spectra at room temperature, though Raman spectra at room temperature are not shown in the figures in this paper. Hiraishi, Taniguchi and Takahashi[20] and Teeters and Frech[21] measured the Raman spectra at room temperature, which is consistent with our results.

The solid lines in Figs. 9–11 are the spectra calculated by the damped harmonic oscillators. Figure 12 shows the temperature dependences of the frequencies and Fig. 13 shows the damping constants (Γ) for the damped harmonic oscillators. In the figures, the librational modes are shown by closed symbols and the translational modes are shown by open symbols. The assignments of the librational and translational modes are followed after Hiraishi, Taniguchi, and Takahashi.[20]

The soft lattice mode related to the phase transition cannot be found in the Raman spectra. However, the phonon frequencies of librational mode vary considerably with temperature. They show a sudden decrease at T_{c2}. And then, they show a slight increase as the temperature approaches T_{c1}. But, a discontinuous jump in the frequency is not found at T_{c1}. Above T_{c1}, they rapidly increase with increasing temperature.

It is interesting to note that the damping constant of each phonon is very large. The damping constant increases suddenly at T_{c2} and is almost constant in the intermediate-temperature phase. In the high-

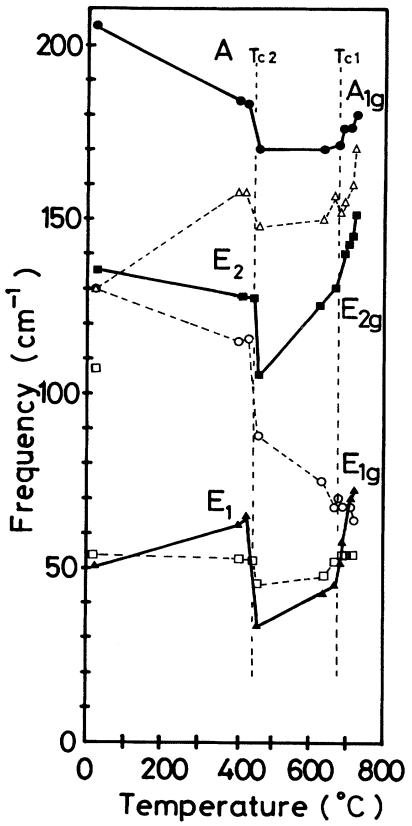

FIG. 12. Temperature dependence of frequency shifts of A_{1g} (circles), E_{1g} (triangles), and E_{2g} (squares) lattice modes measured by Raman scattering of $LiKSO_4$. Librational modes are shown by closed symbols and translational modes are shown by open symbols.

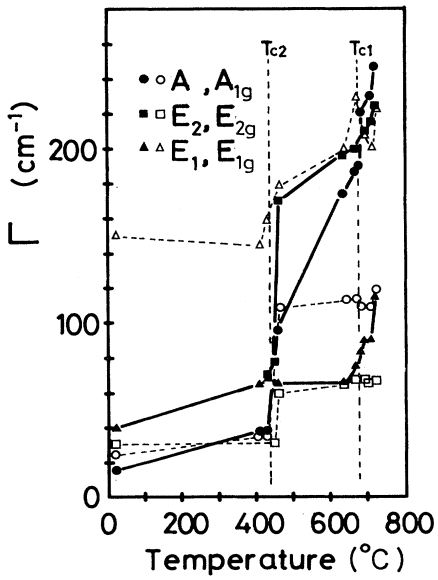

FIG. 13. Temperature dependence of the linewidths Γ of A_{1g} (circles), E_{1g} (triangles), and E_{2g} (squares) lattice modes measured by Raman scattering of $LiKSO_4$. Librational modes are shown by closed symbols and translational modes are shown by open symbols.

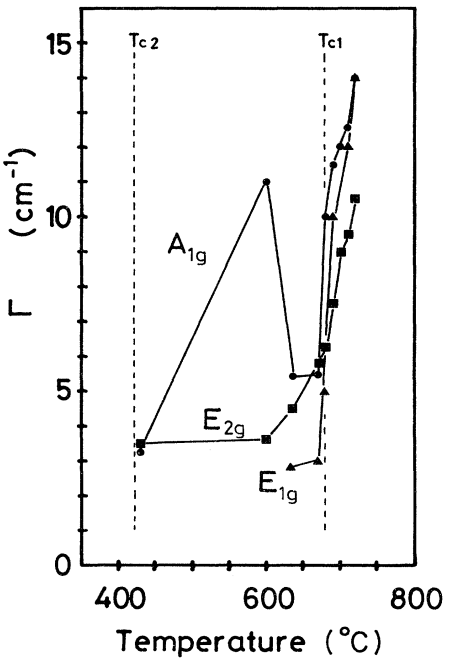

FIG. 14. Temperature dependence of half widths of A_{1g} (circles), E_{1g} (triangles), and E_{2g} (squares) central modes measured by Raman scattering of $LiKSO_4$.

temperature phase, the damping constant of the translational mode is almost constant. However, those of librational modes rapidly increase. A discontinuous jump in the damping constant is not seen at T_{c1}.

The central modes are also seen in Raman scattering in the intermediate- and the high-temperature phases. The solid lines of the central modes in Figs. 9–11 are the Lorentzian line shapes. The half widths of the central modes are shown in Fig. 14. The half widths of E_{1g} and E_{2g} central modes increase smoothly in the intermediate-temperature phase. The central mode of the A_{1g} mode show an unusual temperature dependence. However, the half widths of all central modes rapidly increase in the high-temperature phase. Especially, temperature dependence of full half width of the E_{1g} mode is evident.

IV. DISCUSSION

A. Rotation of SO_4^{2-} tetrahedra in $LiKSO_4$

Various kinds of central mode can be found in $LiKSO_4$ by means of Raman and hyper-Raman scattering. They belong to A_{1g}, E_{1g}, E_{2g}, B_{1u}, and E_{1u} symmetries in the high-temperature phase. These central modes appear in the intermediate- and the high-temperature phases and cannot be found in the room-temperature phase. The half widths are much wider in the high-temperature phase. Thus, these central modes are ascribed to rotational Brownian motions of SO_4 tetrahedra

The tetrahedron of SO_4 ions has the T_d point-group symmetry. The rotational motions of two tetrahedra in a unit cell belong to $2T_1$ modes. These modes split into $2A_2+2E$ modes in C_{3v} site symmetry in which SO_4^{2-} ions are positioned. Further, they split into the space group of $LiKSO_4$, which belongs to C_6 in the room-temperature phase and D_{6h} in the high-temperature phase. Here, one should remember that D_{6h} symmetry of $LiKSO_4$ is supposed for the completely disordered orientation of SO_4^{2-} ions. That is, D_{6h} is the average structure and the crystal structure belongs to the lower symmetries in a moment, according to the orientation of two SO_4 tetrahedra in a unit cell.

In the case of K_2SO_4, which is the isomorphic crystal structure to $LiKSO_4$, it is known[22] by Raman analysis of the internal mode of SO_4^{2-} ions that two types of symmetry exist in a moment and D_{6h} symmetry is an average symmetry. That is, it belongs to C_{6v} symmetry when the tetrahedra order in parallel in a moment. And it belongs to D_{3d} symmetry when they order in antiparallel in a moment.

In the case of $LiKSO_4$, C_{6v} and D_{3d} symmetries would also exist if both compounds are completely isomorphic. However, if SO_4^{2-} tetrahedra tilt about the c axis in $LiKSO_4$, the symmetry becomes lowered from C_{6v} and D_{3d} symmetries.

First, we consider only C_{6v} and D_{3d} symmetries for $LiKSO_4$ for simplicity. Thus, the rotational modes in $LiKSO_4$ split into $B_1+A_2+E_1+E_2$ modes in the case of C_{6v} symmetry and into $A_{1u}+A_{2g}+E_u+E_g$ modes in the case of D_{3d} symmetry. Group theory shows that each mode corresponds to the mode in D_{6h} symmetry, as shown by solid and dashed lines in Fig. 15. Nondegenerate B_{1u} and A_{2g} modes are the rotational modes about the c axis. The rotational motions are shown by the arrows in Fig. 15. Doubly degenerated E_{1u}, E_{2u}, E_{1g}, and

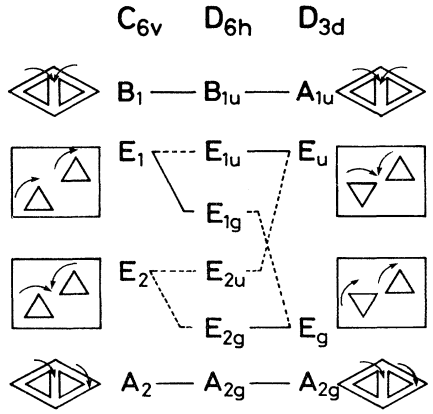

FIG. 15. Schematic diagram of the correspondence of each mode in D_{6h} symmetry to the mode in C_{6v} and D_{3d} symmetries. The rotation of two SO_4 tetrahedra in a unit cell for each mode is also shown.

E_{2g} modes are the rotational modes about the b and c axes. Except for the E_{2u} mode, all the modes are found by Raman and hyper-Raman scattering in our experiment. The E_{2u} mode should be found in hyper-Raman, but it cannot be found. It is assumed that the intensity of this mode may be weak. Because two SO_4^{2-} molecules exist in a unit cell, parallel and antiparallel rotation about the a and b axes exist for C_{6v} and D_{3d} symmetries, as shown in Fig. 15.

Figure 16 shows the temperature dependence of the half widths of E_{1u}, E_{1g}, and E_{2g} central modes in high-temperature phase. One finds that they are different from one another. The half width of the E_{1u} mode is the widest. The half width of the E_{1g} mode is broader than that of the E_{2g} mode in the high-temperature phase. The E_{1g} mode emerges in the vicinity of phase transition temperature T_{c1} in the intermediate-temperature phase and is narrower than the E_{2g} mode in the intermediate-temperature phase. Thus, three sorts of the central modes are found by means of Raman and hyper-Raman scattering. They should belong to the four types of rotational symmetries about the a and b axes, though the last one cannot be found.

Figure 17 shows the linewidth of the B_{1u} and A_{1g} modes. It is surprising that both have the same linewidth. The B_{1u} mode is the rotational mode about the c axis in the antiphase. The A_{2g} mode is the rotational mode about the c axis in the same phase. However, the A_{2g} mode is the silent mode which is all inactive for infrared, Raman, and hyper-Raman measurements.

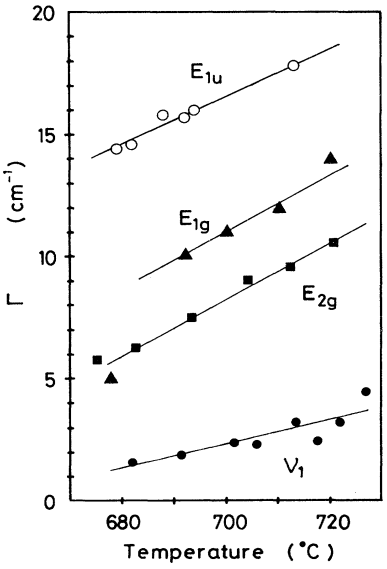

FIG. 16. Comparison of the half widths of the E_{1u}, E_{1g}, and E_{2g} central modes, which are measured by hyper-Raman and Raman scattering. Closed circles are obtained from the difference of the linewidth between the polarized and depolarized Raman spectra of the ν_1 internal mode.

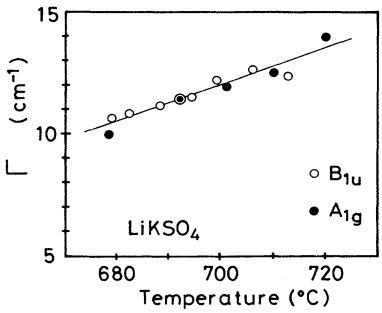

FIG. 17. Comparison of the half widths of the B_{1u} and A_{1g} central modes, which are measured by hyper-Raman scattering and Raman scattering.

This mode is only active for the second hyper-Raman scattering. (Second hyper-Raman scattering of $LiKSO_4$ was measured, but it is too weak to be observed in our measurement.) On the other hand, the A_{1g} mode is not the rotational mode which cannot be obtained in the D_{3d} and C_{6v} symmetries. However, the A_{1g} mode is the rotational mode in D_3 symmetry, which is distorted from D_{3v} symmetry by tilting the SO_4 tetrahedra about the c axis.

Rotations about the a and b axes have various modes. This fact suggests that the correlation of SO_4 tetrahedra in a unit cell is strong or the correlation between SO_4-tetrahedra rotation and Li-ion conduction is strong. It is clear that the rotations of two tetrahedra in antiphase are easy, because the rotation of a tetrahedron can help another rotation. When they rotate in phase, this rotation of one tetrahedron disturbs another. This is the reason why the linewidths of the rotational mode about the a and b axes are different from each other.

On the contrary, the rotation of tetrahedra about the c axis seems not to have strong correlation, because the heights of two tetrahedra are different along the c axis in a unit cell and do not have strong correlations between them.

We assign each mode in D_{6h} symmetry to the rotations in C_{6v} and D_{3d} symmetries, as shown by the solid lines in Fig. 15. The E_{1u} mode may be due to the E_u mode in D_{3d} symmetry, because this is the fastest mode and the tetrahedra rotate in antiphase. The E_{1g} and E_{2g} modes may be due to the rotations in phase. Thus, the E_{1g} and E_{2g} modes correspond to the E_1 and E_g modes in C_{6v} and D_{3d} symmetries, respectively.

The temperature dependence of the A_{1g} mode in the intermediate-temperature phase is curious, as shown in Fig. 14. Though the detailed temperature dependence of this mode is not obtained, the linewidth around 600 °C is extremely wide. This fact may suggest that the partial disorder of SO_4^{2-} tetrahadron rotation in the intermediate-temperature phase is caused by the rotation about the c axis.

Chaplot and Rao[23] calculated the molecular dynamics of the rotational motions of SO_4^{2-} ions in $LiKSO_4$. They concluded that the half width of the rotational mode is

about 3 cm^{-1} at around 1000 K. This result is consistent with our result, though it is somewhat narrower than ours. They also concluded that the rotations about the c axis are twice as probable as the rotations about the a and b axes below 1000 K. Above 1000 K, rotations about all axes have nearly equal probability. However, in our results, the rotations about the a and b axes have various modes and the rotation in the E_{1u} mode is always faster than that about the c axis. The rotation in the E_{2g} mode is slower than that about the c axis. It is thought that correlations between SO_4^{2-} molecules or the coupling between Li^+-ion conduction and SO_4^{2-}-tetrahedron rotation will be of crucial importance in a detailed calculation of the molecular dynamics.

B. Coupling mechanism between lithium-ion conduction and SO_4^{2-}-tetrahedron rotation

If the paddle-wheel mechanism is applicable, the hopping of lithium ions is assisted by the SO_4-tetrahedra rotation. Among rotations about the a and b axes, the rotation belonging to the E_{1u} symmetry is the fastest. Lithium-ion hopping along the c axis may be mainly due to this mode in the high-temperature phase. On the other hand, lithium-ion hopping in the a-b plane may be due to rotations about the c axis belonging to a B_{1u} mode. The ratio of relaxation times between the E_{1u} and B_{1u} modes is determined to be about 1.38 from Fig. 8,

$$\Gamma_{E_{1u}}/\Gamma_{B_{1u}}=\tau_{\parallel}/\tau_{\perp}=1.38 ,$$

where $\tau_{\parallel}=1/\Gamma_{B_{1u}}$ is the rotational relaxation time about the c axis and $\tau_{\perp}=1/\Gamma_{E_{1u}}$ is the rotational relaxation time about the a and b axes. One finds that this ratio is very close to the ratio of the conductivities $\sigma_{\parallel}/\sigma_{\perp}=1.28$. Therefore, this fact suggests that SO_4^{2-}-tetrahedron rotation is very closely related with the ionic conduction of Li^+ ions.

Considering the crystal structure of $LiKSO_4$, the hopping of Li^+ ions may be assisted by the SO_4^{2-}-ion rotation, as shown in Fig. 18. Here, two characteristic times are frequently employed to characterize the ionic conductivity: the flight time (τ_f), which is the time spent for the transit between two sites, and the residence time (τ_r), which is the inverse of the attempt frequency.

When the residence time τ_r is longer than τ_f, the lithium-ion hopping is thermally activated by the rotation of SO_4 ions. That is, SO_4 rotation can be considered as a kind of attempt frequency. The ratio of the conductivities is obtained, as follows:

$$\sigma_{\parallel}/\sigma_{\perp}=(1/\tau_{\perp})/(1/\tau_{\parallel})=1.38 .$$

When flight time τ_f is longer than τ_r, the lithium-ion hopping rate is proportional to the velocity (v)of migration. In this model, the ratio of the conductivities is obtained as follows:

$$\sigma_{\parallel}/\sigma_{\perp}=v_{\parallel}/v_{\perp}=(l_{\parallel}/\tau_{\perp})/(l_{\perp}/\tau_{\parallel})=1.13 ,$$

where $l_{\parallel}=4.353$ Å and $l_{\perp}=5.295$ Å in $LiKSO_4$.[8] By this model, lithium-ion migration in $LiKSO_4$ is rather similar to the motion of liquid molecules.

Since the value of ratio $\sigma_{\parallel}/\sigma_{\perp}=1.28$ is in the middle of both ratios, $LiKSO_4$ is in the middle of both types.

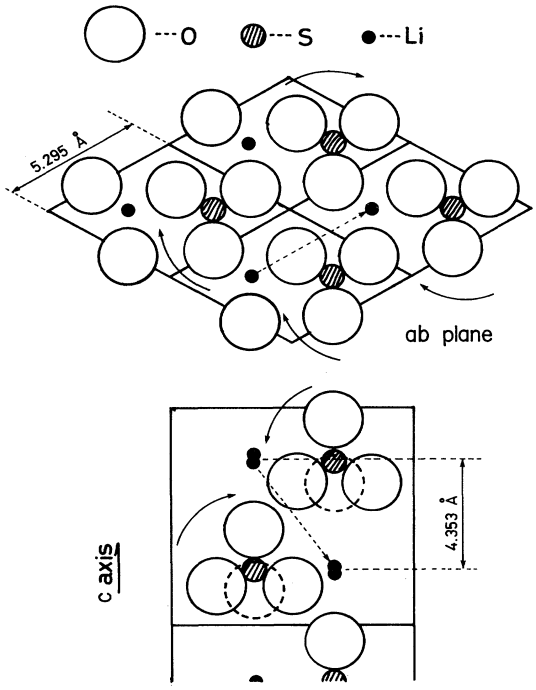

FIG. 18. Way of lithium-ion conduction coupled with SO_4 rotation.

C. Comparison between the central mode and the line broadening of SO_4^{2-} internal modes

Borjesson and Torell[24] measured the linewidth of the totally symmetric ν_1 internal mode for Li_2SO_4 and $LiAgSO_4$. They show the reorientational relaxation time is derived from the deviation of anisotropic linewidths of the internal modes. Thus, we also measured the anisotropic linewidth of the ν_1 internal mode for $LiKSO_4$. An example of the internal mode which was measured at 725°C are shown in Fig. 19. The linewidth of the polarized spectrum is about 24.6 cm^{-1}. In the case of depolarized spectra, ν_1 mode should be forbidden. However, the ν_1 mode is found in the depolarized spectrum, like the other sulfate crystals of Li_2SO_4 and $LiAgSO_4$.[24] The spectra of the internal mode of $LiKSO_4$ are very similar to those spectra. The depolarized spectrum is deconvoluted by the ν_1 and ν_3 spectra, as shown by the solid line in Fig. 19. The dashed line in Fig. 19 is the ν_3 mode and the solid line is the ν_1 mode. The linewidth of the ν_1 mode in depolarized spectra is obtained to be 30.2 cm^{-1}. If the analysis is followed after Borjesson and Torrell, the difference of the linewidths is due to the rotational motion of SO_4^{2-} ions. However, this result is far narrower than the results obtained by the central modes in this study.

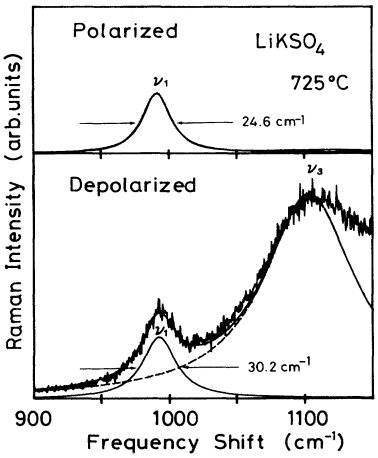

FIG. 19. Polarized and depolarized Raman spectra of ν_1 internal modes of $LiKSO_4$.

The temperature dependence of the difference of the ν_1 linewidth is shown by closed circles in Fig. 16. The results are much narrower than the linewidth of the E_{1u}, E_{1g}, and E_{2g} modes, though they also increase at high temperature.

Their analysis is based on the study[25] of the internal mode of CCl_4 liquid. Therefore, this analysis can be applied to the ν_2 and ν_4 internal modes, but cannot be applied to the totally symmetric ν_1 mode. Thus, it is supposed that such analysis cannot be applied to sulfate crystals, because anisotropy in the linewidth broadening are found in the ν_1 mode and cannot be found in the ν_2 and ν_4 modes.

However, the ν_1 mode is weakly seen in the depolarized spectra even in the CCl_4 liquid,[26] though this mode is forbidden in the depolarized scattering configuration. This spectrum is due to the intermolecular interactions. The forbidden mode in the depolarized ν_1 mode which is seen in $LiKSO_4$ may be due to the interactions between the SO_4 tetrahedra or the interactions between Li-ion migration and SO_4 rotation. The temperature dependence of the linewidth of the ν_1 mode may show that such interactions increase at high temperature.

IV. CONCLUSION

Central modes due to the rotational Brownian motion of SO_4^{2-} tetrahedra about the c axis are measured in A_{1g} and B_{1u} modes. The B_{1u} mode is the silent central mode, which has been observed in the present work. The rotational modes about the a and b axes are measured in E_{1u}, E_{1g}, and E_{2g} modes. Each central mode is assigned to the rotational motions of two SO_4^{2-} tetrahedra in a unit cell. In the rotational modes about the a and b axes, the interactions between the SO_4^{2-} tetrahedra are found to be strong.

The anisotropy of lithium-ion conduction is well elucidated by the ratio of the relaxation times of B_{1u} and E_{1u} modes. This fact strongly supports the paddle-wheel mechanism. That is, lithium-ion migration along the c axis is assisted by SO_4 rotation about the a and b axes (E_{1u} mode) and the lithium-ion migration in the ab plane is due to the rotation about the c axis (B_{1u} mode). However, although the linewidth of the ν_1 internal mode seems to be related to SO_4^{2-} interactions, it does not appear directly related to the rotational relaxation times.

[1]A. Lunden and J. O. Thomas, in *High Conductivity Solid Ionic Conductors: Recent Trends and Applications,* edited by T. Takahashi (World Scientific, Singapore, 1986).
[2]L. Nilsson, J. O. Thomas, and B. C. Tofield, J. Phys. C **13**, 6441 (1980).
[3]M. Karppinen, Jan-Olof Lundgren, and R. Liminga, Acta Crystallogr. Sect. C **39**, 34 (1983).
[4]P. E. Tomaszewski and K. Lukaszewicz, Phase Transit. **4**, 37 (1983).
[5]R. Cach, P. Tomaszewski, P. Bastie, and J. Bornarel, Ferroelectrics **53**, 337 (1984).
[6]Y. Y. Li, Solid State Commun. **51**, 355 (1984).
[7]S. Bhakay-Tamhane, S. Sequeira, and R. Chidambaram, Acta Crystallogr. Sect. C **40**, 1648 (1984).
[8]H. Schultz, U. Zucker, and R. Frech, Acta Crystallogr. Sect. B **41**, 21 (1985).
[9]T. Krajewski, T. Breczwski, P. Piskunowicz, and B. Mroz, Ferroelect. Lett. **4**, 95 (1985).
[10]S. Bhakay-Tamhane, A. Sequeira, and R. Chidambaram, Solid State Commun. **53**, 197 (1985).
[11]A. M. Balagurov, B. Mroz, N. C. Popa, and B. N. Savenko, Phys. Status Solidi A **96**, 25 (1986).
[12]B. Bhakay-Tamhane and A. Sequeira, Ferroelectrics **69**, 241 (1986).
[13]A. Pietraszko, Ferroelectrics **79**, 121 (1988).
[14]R. H. Chen and R. T. Wu, J. Phys. Condens. Matter **1**, 6913 (1989).
[15]A. J. van den Berg, and F. Tuinstra, Acta Crystallogr. Sect. B **34**, 3177 (1984).
[16]M. A. Pimenta, P. Echegut, Y. Luspin, G. Hauret, and F. Gervais, Phys. Rev. B **39**, 3361 (1989).
[17]M. A. Pimenta, P. Echegut, and F. Gervais, Solid State Ion. **28-30**, 224 (1988).
[18]S. Shin and M. Ishigame, J. Chem. Phys. **89**, 1892 (1988).
[19]S. B. Kim and R. Frech, J. Chem. Phys. **88**, 2216 (1988); E. Cazzzanelli and R. Frech, *ibid.* **79**, 2615 (1983).
[20]J. Hiraishi, N. Taniguchi, and H. Takahashi, J. Chem. Phys. **65**, 3821 (1976).
[21]D. Teeters and R. Frech, Phys. Rev. B **26**, 5897 (1982).
[22]M. Ishigame and S. Yamashita, Phys. Status Solidi B **116**, 49 (1983).
[23]S. L. Chaplot and K. R. Rao, Phys. Rev. B **35**, 9771 (1987).
[24]L. Borjesson and L. M. Torell, Phys. Rev. B **32**, 2471 (1985); Solid State Ion. **18&19**, 582 (1986).
[25]S. Sunder and R. E. D. MaClung, Chem. Phys. **2**, 467 (1973); F. J. Bartoli and T. A. Litovitz, J. Chem. Phys. **56**, 413 (1972).
[26]S. Hyodo and T. Fujiyama, Bull. Chem. Soc. Jpn. **63**, 2456 (1980).